Nanoscale

COMMUNICATION

View Article Online
View Journal | View Issue

Cite this: *Nanoscale*, 2026, **18**, 9618

Received 5th February 2026,
Accepted 29th March 2026

DOI: 10.1039/d6nr00513f

rsc.li/nanoscale

Nanowire photodetectors: path to single physical artificial neurons

Yunqiu Chen,† Milad Fathabadi,† Mohammad Fazel Vafadar and Songrui Zhao *

Neurons are basic units for information processing in biological systems. Inspired by the information-processing efficiency of biological systems, artificial neural networks (ANNs) have been studied for decades. However, it remains challenging today to realize single physical artificial neurons so that an ANN can be constructed in a bottom-up manner. Herein, we show that by using an innovative light-detecting semiconductor nanowire structure, neuronal features much closer to single, physical artificial neurons can be emulated, including excitation and inhibition, threshold, refractory period, and temporal summation. The analogy between the presented neuron-like nanowire photodetectors and neurons in the human retina system is also discussed. This study lays the cornerstone for the bottom-up construction of a physical ANN.

Introduction

Despite the exciting progress with artificial intelligence, which has improved our everyday lives considerably, the ANNs we are dealing with today are based either on mathematical functions or large-scale circuitry that model the behavior of biological neuronal systems, rather than being constructed from single physical artificial neurons.[1–10] This is because single artificial neurons have yet to be achieved. Fig. 1a illustrates the basic structure of a neuron (axodendritic kind), including the axon, which functions as the primary output pathway, and the dendrite, which receives the input from other neurons. These structures communicate at the synaptic cleft – a specialized junction that facilitates interneuronal communication. Signal transmission across the synaptic cleft is mediated by neurotransmitters (chemical messengers) released from the presynaptic neuron. The type of synapse between neurons (excitatory or inhibitory), along with the strength and properties of the presynaptic and the postsynaptic neurons, is highly critical for information processing in such a neural network.[11]

To achieve single physical artificial neurons, one must demonstrate a small-scale device roughly the size of typical neurons (*e.g.*, tens of μm) that does not rely on large-scale circuits and can emulate as many neuronal features as possible, such as temporal summation, excitation, inhibition, threshold, and refractory period. In recent years, we have witnessed an increasing number of studies using semiconductor devices to emulate neurons. However, constrained by their physical properties, existing semiconductor devices can only emulate limited neuronal features and thus do not yet closely resemble single physical neurons. For example, existing studies can only emulate excitation and temporal summation but cannot reproduce inhibition, threshold, and refractory period simultaneously.[12–16]

In this study, we demonstrate an innovative semiconductor nanowire photodetector based on a nanowire ensemble that can emulate features much closer to single, physical neurons (Fig. 1b). Thanks to the rich photoresponse of the presented device, rich neuronal features, including excitation, inhibition, threshold, refractory period, and temporal summation, can be emulated. The rich photoresponse demonstrated in the present semiconductor device has not been achieved previously. In the present study, the very rich photoresponse is made possible by leveraging the unique physical properties of semiconductor III-nitrides, including wide-range optical bandgap tunability that can tune the photoabsorption properties, excellent strain relaxation in nanowires that allow highly flexible material stacking with a minimum penalty from lattice mismatch, and careful engineering of device layers, such as the choice of materials and alloy composition. The operating voltage for such devices is only tens of millivolts, significantly lower than the previously reported devices (several volts to tens of volts), which can only emulate some neuronal features.[15,16]

Department of Electrical and Computer Engineering, McGill University, 3480 University Street, Montreal, Quebec H3A 0E9, Canada.
E-mail: songrui.zhao@mcgill.ca; Tel: (+1) 514-398-3244
†Y. C. and M. F. contributed equally to this work.

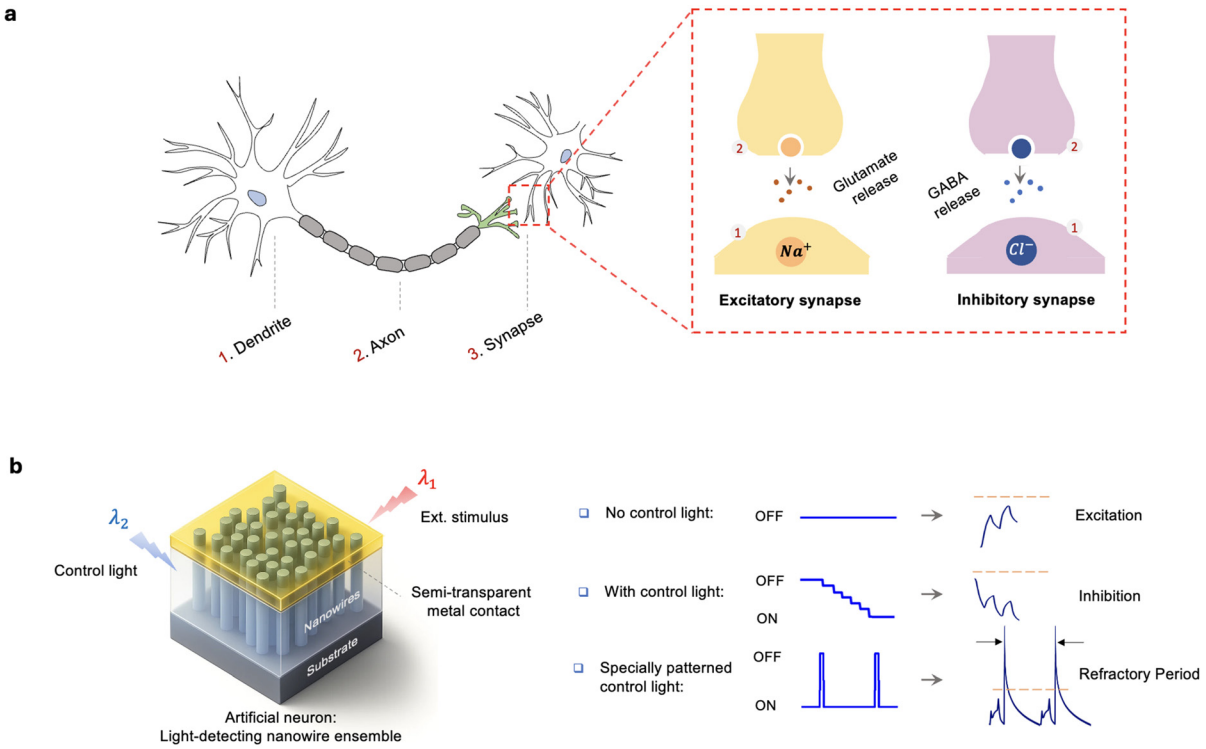

Fig. 1 Illustration of the presented neuron-like nanowire photodetectors. (a) Neurons in biological systems. (b) Schematic of the neuron-like nanowire photodetectors in this study. The right panel illustrates how to emulate different neuronal characteristics using the control light. The dashed line denotes the action potential threshold.

Structural properties of the light-detecting nanowires

Fig. 2a illustrates the layer-by-layer structure of the individual nanowire obtained using energy dispersive X-ray spectroscopy (EDXS) imaging. Each layer is clearly visible and labeled. Such a structure is denoted as a PNNP structure. A scanning electron microscopy (SEM) image of a nanowire ensemble is shown in Fig. 2b. It is seen that nearly vertically aligned nanowires are formed. Such nanowires are formed in a self-assembled manner, without any additional processes such as substrate patterning. The nanowires also have excellent interface quality, especially at the n-GaN/n-AlGaN interface, which is critical to this study. Additional electron microscopy studies can be found in SI Note 1.

The alloy compositions of the layers were examined using room-temperature photoluminescence spectroscopy (RTPL). The details can be found in SI Note 2. To summarize here, the p-InGaN layer absorbs 405 nm blue incident light (used as the control light), and 266 nm ultraviolet (UV) light (used as the external stimulus) is absorbed by both the p-InGaN and n-GaN layers.

Photocarrier dynamics

Fig. 2c illustrates the energy band diagram of the PNNP structure. Under UV light illumination, although both the GaN and p-InGaN layers absorb the light, due to the large band offset at the n-AlGaN/p-InGaN interface and the presumably better light absorption of the GaN layer compared to the InGaN layer due to the greater thickness, a net positive photocurrent is generated.[17] It is important to note that, different from thin films in which the light path has to be vertical, in nanowires, the light can be scattered to the nanowire root and absorbed. Moreover, further examining the n-GaN/n-AlGaN interface, the downward band bending on the n-GaN side traps electrons. This is also illustrated in Fig. 2c. Due to the electron trap, when the light is turned off, the slow release of the trapped electrons contributes to a persistent positive photocurrent, whereas when the light is turned back on, the photocurrent continues to increase, as illustrated in Fig. 2d.

The charge trap at the n-GaN/n-AlGaN interface also produces a rich photoresponse under blue light stimulation. In this case, the light is only absorbed by the p-InGaN layer, and thus a negative photocurrent is generated. However, due to the trapped electrons at the n-GaN/n-AlGaN interface (n-GaN side), a positive current spike appears immediately when the blue light is turned off with a small bias voltage (~50 mV) applied, as illustrated in Fig. 2e. This small, applied bias is to overcome the potential barrier for the charge carrier transport. As the charge accumulation takes time, the longer that the blue light is kept on before being turned off, the larger the positive photocurrent spike will be; whereas when the blue light is chopped frequently, the positive photocurrent spike is noticeably smaller, as illustrated in the inset of Fig. 2e.

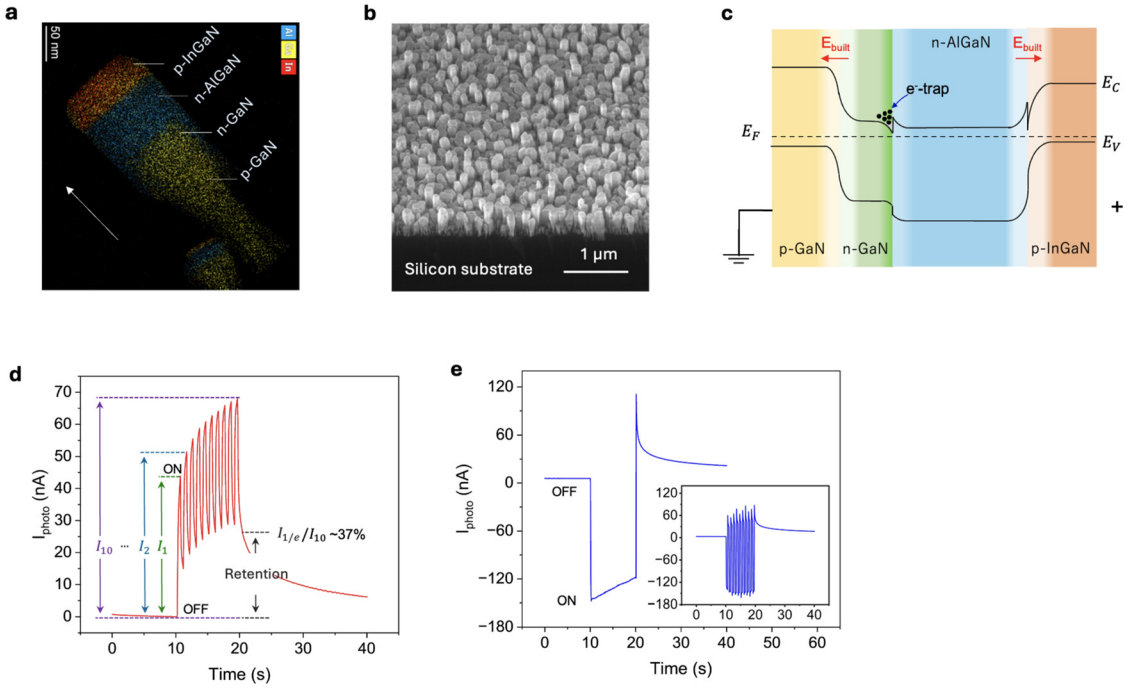

Fig. 2 Structural properties and mechanism of photocarrier control. (a) EDXS imaging performed in dark-field STEM mode. The arrow denotes the growth direction. (b) SEM image of a nanowire ensemble. (c) Schematic of the energy band diagram of the PNNP structure. The Si substrate is on the left side (not shown). (d) Time-dependent photocurrent under UV light illumination (average power of 3 mW cm^{-2}) and 50 mV bias voltage. Other notations are discussed in the main text. (e) Time-dependent photocurrent under blue light illumination (0.32 W cm^{-2}) and 50 mV bias voltage. Inset: Time-dependent photocurrent when the blue light is turned on and off frequently.

In this study, the charge trapping effect at the n-GaN/n-AlGaN interface is also examined for the comparison nanostructure (PNP), wherein the n-GaN layer between p-GaN and n-AlGaN is removed (and thus the electron trap is removed). In this case, the temporal summation of the positive photocurrent under the UV light illumination disappears. More details about the comparison between the PNNP and PNP structures can be found in SI Notes 3 and 4.

Neuron-like characteristics

Here, we will describe how to use the presented semiconductor nanowire photodetectors to emulate various neuronal features. Excitation is described first. In this case, one can simply turn off the blue control light or modulate (*i.e.*, on and off) the control light frequently. The time-dependent photocurrent of the former is shown in Fig. 2d, whereas for the latter it is shown in Fig. 3a (light profiles) and 3b (light response). In either case, treating the time-dependent photocurrent as the time-dependent postsynaptic potential in the postsynaptic neuron, excitation can be seen, *i.e.*, the membrane potential in the postsynaptic neuron is more positive and thus has an increased likelihood of firing. Moreover, when a pulse train is used (*i.e.*, the UV light is repeatedly turned on and off), the consecutive pulse generates a higher photocurrent compared to the previous pulse. This mimics pulse-number-dependent plasticity (and here, it is facilitation), *i.e.*, the consecutive pulse generates a higher membrane potential in the postsynaptic neuron compared to the previous pulse, and could be treated as short-term plasticity.[18–20] Temporal summation is also seen, *i.e.*, successive input signals add up.

We next consider inhibition. In this case, as the control light leads to a negative photocurrent (when it is turned on), one can utilize this feature to introduce inhibition. For example, when the light intensity of the control light is increased continuously (Fig. 3c), the time-dependent photocurrent decreases under each consecutive pulse of the UV light (Fig. 3d). This could emulate inhibition of neurons, namely, a more negative membrane potential in the postsynaptic neuron and thus a reduced likelihood of firing. Moreover, when the input signal is a pulse strain, pulse-number-dependent plasticity is also seen (and in this case, it is depression). Furthermore, just like excitation, temporal summation is also seen for inhibition, *i.e.*, successive input signals add up, although it is a decrease. It is further noted that: (1) simply reducing the UV light could also reduce the photocurrent under consecutive pulses, and we consider it as a trivial case; (2) the purpose of the control light is to reduce the photocurrent; as such, the choice of light intensity profile of the control light can be highly flexible. Essentially, the change of the control light may mimic the release of neurotransmitters (*e.g.*, glutamates or gamma-aminobutyric acid [GABA], as shown in Fig. 1a). However, it needs to be made clear that,

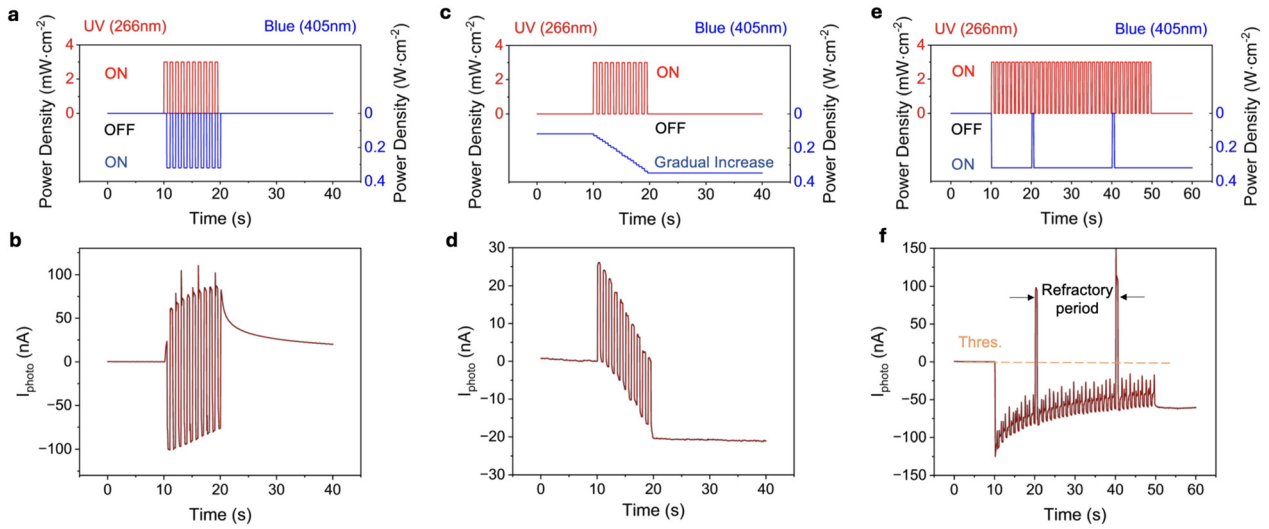

Fig. 3 Detailed characteristics of the presented neuron-like nanowire photodetectors. (a) Light intensity profiles for excitation, and (b) photocurrent profile that emulates excitation. (c) Light intensity profiles for inhibition, and (d) photocurrent profile that emulates inhibition. (e) Light intensity profiles for threshold and refractory period, and (f) photocurrent profile that emulates the threshold and refractory period. For (b) and (f), the applied bias is 50 mV, and for (d), the applied bias is 10 mV.

different from typical biological neurons wherein such control is coded in a protein inside the neuron, the blue control light here is external to the artificial neuron.

Lastly, we consider emulating the threshold and refractory period related to spiking neurons. For spiking neurons, an action potential can be fired when the membrane potential exceeds the threshold. In this case, at least four key features need to be shown: (1) attempt to fire, *i.e.*, an increase of membrane potential, (2) firing action potential (a pulse signal), (3) reset, and (4) refractory period, *i.e.*, neurons cannot fire again even if the stimulus is present.[3] To emulate these features, one can use the control light profile as shown in Fig. 3e, *i.e.*, on with brief off. The time-dependent photocurrent is shown in Fig. 3f, which can emulate attempts to fire (small photocurrent spikes), firing action potential (a large photocurrent spike), reset (the photocurrent drops back to baseline), and refractory period (gap between two large photocurrent spikes). It is also noted that pulse-number-dependent facilitation is also evident here between each fire, similar to Fig. 2d and 3b.

More analysis on pulse-number-dependent facilitation

The facilitation index is analyzed first. In this regard, as the plasticity is associated with the positive photocurrent under UV light stimulus, the blue control light was not used. The facilitation index under a pulse train is measured by the photocurrent difference between two consecutive light pulses, *i.e.*, $(I_{n+1} - I_n)/I_n$, where I_n is the photocurrent under the n^{th} light stimulus (as denoted in Fig. 2d). Fig. 4a shows the facilitation index *versus* each stimulus under different applied bias voltages. It is seen that the facilitation index is less sensitive to bias.

This is an important feature, meaning the presented neuron-like nanowire photodetectors can "learn" with very low power consumption. In contrast, for the previously demonstrated devices, much larger voltages (several volts to tens of volts) are required to operate, meaning significantly higher power consumption.[16,21,22] Moreover, as the power efficiency of III-nitride semiconductor light sources can be higher than 50%, *e.g.*, ref. 23, this means that even considering the power consumption of the additional light source for operating such devices, the overall power consumption remains significantly lower compared to those operated by large applied bias voltages.

Fig. 4b further demonstrates the facilitation index under different excitation powers, and in this case, it is seen that a higher excitation power leads to a smaller facilitation index (a lower degree of facilitation). Moreover, it is seen that whether in the voltage dependence (Fig. 4a) or the excitation power dependence (Fig. 4b), the facilitation index reduces as the pulse number increases.

The synaptic strength increase is also studied as a function of pulse numbers, *i.e.*, 10, 20, 40, and 80, for four different pulse trains. Fig. 4c shows the corresponding photocurrent under the same experimental conditions. The grey line is a fitting curve using the Hill function:

$$f_{\text{Hill}}(t) = \frac{a \cdot t^m}{k^m + t^m} \quad (1)$$

wherein t denotes the time interval, and k and m are the apparent dissociation constant and the Hill constant, respectively. An R_{square} value of 0.9971 is obtained, confirming excellent fitting using eqn (1). The fitted residual photocurrent is

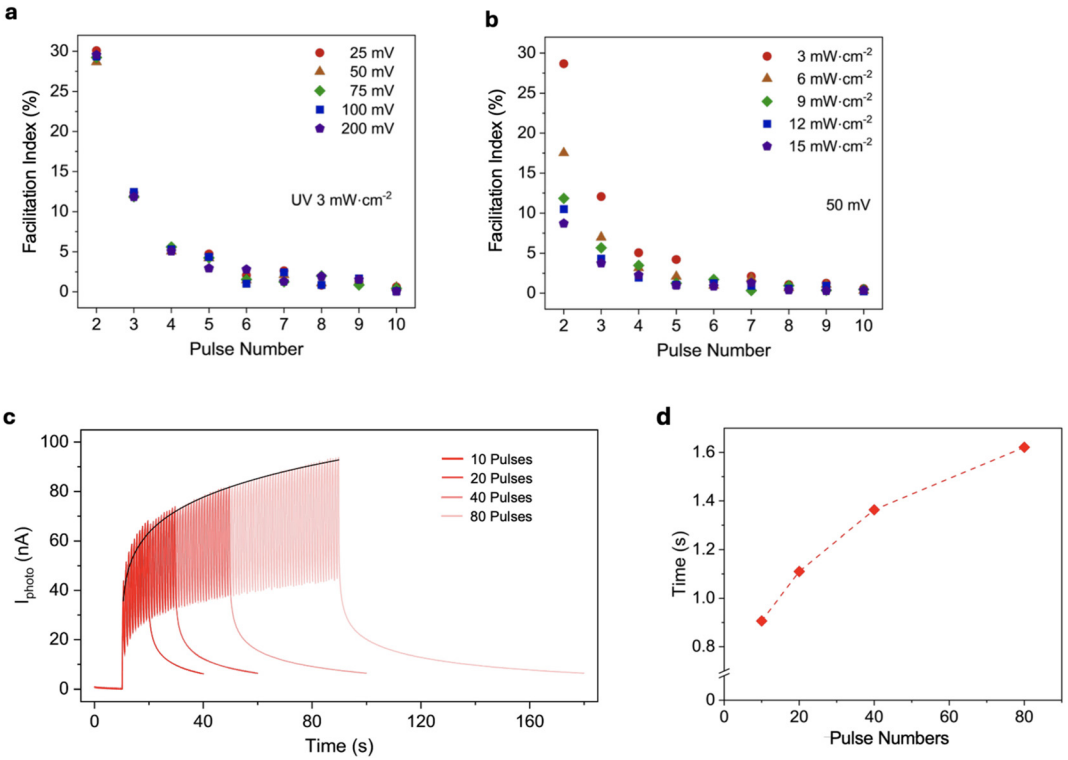

Fig. 4 More analysis on pulse-number-dependent facilitation. (a and b) Facilitation index *versus* each stimulus under different applied bias voltages and under different excitation powers, respectively, as denoted in Fig. 2d. (c) Photocurrent profiles *versus* pulse numbers. (d) Time of synaptic strength decay *versus* pulse numbers. More details are described in the main text. For (c) and (d), the applied bias is 50 mV, and the UV light average power density is 3 mW cm^{-2}.

plotted in Extended Data Fig. 5. It is seen that the synaptic strength increase follows the Hill function very well, and the synaptic strength can be predicted even at large pulse numbers, rooted in the excellent stability of the presented device.

Finally, synaptic strength decay *versus* pulse number is studied. In this case, we consider the synaptic strength increase after the end of each pulse train and examine the decay time when the photocurrent is reduced to ~37% (1/*e*, a natural decay is considered) of the value before the pulse train ends. For example, when the pulse number is 10, we examine the time at $I_{1/e}$ when $I_{1/e}/I_{10} \sim 37\%$, as illustrated in Fig. 2d. The moment when the pulse train ends is set as 0 s. It is seen that, with a larger pulse number, the decay time increases, and close to 2 s is obtained with a pulse number of 80. This mimics the learning process in typical biological neuron systems in the sense that with more rehearsals, the plasticity lasts longer.

Analogy to artificial retina

The top panel of Fig. 5a illustrates the working principle of a human retina: briefly, photoreceptors such as cones and rods convert the optical signal into an electric signal, which forms synapses on bipolar cells. Bipolar cells can be either excitatory or inhibitory, and form synapses on ganglion cells, which fire action potentials to the optic nerve when the threshold is reached. This allows further optical information processing in the primary visual cortex or other regions of the brain for high-level processing, such as object distinction, scene segmentation, and so on.[24] Neurons in the retina can also pre-process certain visual information, such as enhancing the image contrast and the signal-to-noise ratio.[25–28]

The presented neuron-like nanowire photodetectors can mimic, to some extent, the photoreceptors – bipolar cells – ganglion cells ensemble. As shown in Fig. 3f, the presence of synaptic plasticity could emulate the plasticity of bipolar and ganglion cells, and the action potential firing in Fig. 3f could emulate the firing of ganglion cells to the optic nerves. As such, the presented neuron-like nanowire photodetectors could be readily used to build an artificial retina. Fig. 5b shows an overview of using the presented neuron-like nanowire photodetectors to construct a conceptual artificial retina. Briefly, artificial red (R), green (G), and blue (B) cells (can be more cells) detect light and pre-process light information. By further introducing optics and electronics and combining with external convolutional neural networks (CNNs) of various specific functions, complex visual information can be processed.

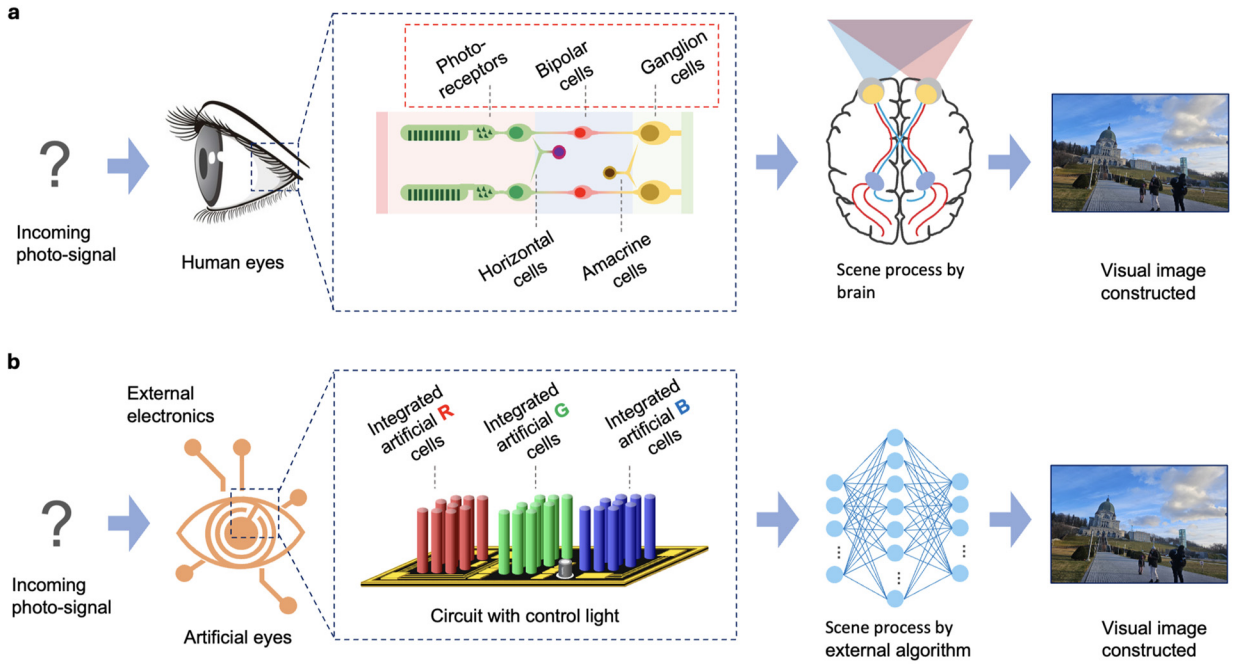

Fig. 5 Analogy of the presented neuron-like nanowire photodetectors to the human retina. (a) Illustration of the working principle of the human retina. (b) Illustration of the concept using the presented neuron-like nanowire photodetectors for retina-like imaging.

Discussion and outlook

As the size and the density of the nanowires can be controlled using selective area epitaxy,[29–31] the presented neuron-like nanowire photodetectors can have a preset synaptic strength, allowing them to mimic the specific colour sensitivity that different species have developed through evolutionary processes. Using selective area epitaxy further allows us to design artificial sensors with multiple focus zones, mimicking multiple foveae in birds.[32–34] In addition, leveraging the widely tunable bandgap of III-nitrides, which ranges from near-infrared to deep ultraviolet,[35–37] the optical response of such an artificial retina can be extended beyond RGB.

Methods

Nanowire epitaxial growth

The light-detecting nanowires were grown on n-type Si (111) substrates using plasma-assisted molecular beam epitaxy (MBE). The growth began with a thin n-GaN nanowire layer to mitigate the electrical mismatch between n-Si and p-GaN. This was followed by the sequential growth of p-type GaN, n-type GaN, n-type AlGaN, and p-type InGaN segments in the format of nanowires. Magnesium (Mg) and silicon (Si) were p-type and n-type dopants, respectively. For n-type doping, the Si cell temperature ranged from 1100 °C to 1200 °C, while for p-type doping, the Mg cell temperature was between 280 °C and 300 °C. These conditions correspond to doping concentrations of approximately 10^{18}–10^{19} cm^{-3}.[17,38–43] The GaN, AlGaN, and InGaN segments were grown at substrate temperatures of 740 °C, 830 °C, and 590 °C, respectively. For GaN, a nitrogen flow rate of 1.5 sccm and a Ga beam equivalent pressure (BEP) of approximately 7×10^{-8} Torr were used. For AlGaN, the nitrogen flow rate was 0.9 sccm, and Ga and Al BEPs were 2.4×10^{-8} Torr and 1.7×10^{-8} Torr, respectively. The InGaN layer was grown with Ga and In BEPs of 2.4×10^{-8} Torr and 2.2×10^{-8} Torr, respectively, under a nitrogen flow rate of 0.9 sccm.

Device fabrication

The neuron-like nanowire photodetectors were fabricated by standard photolithography and metallization techniques. The p-contact, which defines the device size (1 mm × 1 mm in this study), was formed by depositing a Ni/Au bilayer (15/15 nm) on the top surface of the nanowires. The n-contact was established by applying colloidal silver (Ag) paste to the backside of the highly conductive n-Si substrate. Importantly, it is noted that the p-contact size can be further reduced, and in fact, a p-contact size as small as 1 μm × 1 μm is possible.[44,45] Therefore, the presented nanowire photodetectors offer a viable path towards single artificial neurons, significantly different compared with using large-scale circuits to emulate neuronal dynamics. In this study, an example photoresponse from a 300 μm × 300 μm device is shown in the SI.

Device characterization

The optoelectronic properties of the neuron-like nanowire photodetectors were characterized using Keithley 2400 source meter units (SMUs). The devices were placed on an Al plate, with the colloidal Ag paste applied underneath. The ground probe from the SMU was connected to the Al plate, while the

voltage biasing probe contacted the metal pad of the device. Light from the sources was focused onto the devices using focus lenses, with an area of ~1 mm^2. The 405 nm blue light (laser) is continuous-wave (CW), whereas the 266 nm UV light (laser) is pulsed. Note that the meaning of pulse here is an intrinsic property of the laser, whereas the pulse mentioned in the main text refers to periodic on/off light. A calibrated Si photodiode was used to measure the incident light intensity.

Electron microscopy

The SEM images were taken using a field-emission (FE) SEM. The wafers were tilted at a 45-degree angle. To study the structural properties, TEM analysis was carried out using a Tecnai Talos F200× G2 TEM. The nanowires were mechanically transferred onto a TEM grid.

Author contributions

S. Z. conceived the idea and directed the project. Y. C. and M. F. performed device characterizations. Y. C. performed experiments on neuron emulation. M. V., S. Z., and M. F. performed the MBE growth of the nanostructures. S. Z. and M. V. performed the electron microscopy experiments. M. V. fabricated the devices. S. Z. wrote the manuscript, with comments from all authors.

Conflicts of interest

The authors declare no competing financial interest.

Data availability

The data supporting this article have been included as part of the supplementary information (SI). Supplementary information: additional electron microscopy studies; alloy composition of the light-detecting nanowires; comparison with the reference structure and more discussions on the photocarrier dynamics; additional analysis on Hill function fitting; photoresponse of smaller devices; microscope image of the fabricated wafer. See DOI: https://doi.org/10.1039/d6nr00513f.

Acknowledgements

This work is supported by Natural Sciences and Engineering Research Council of Canada (NSERC) and Fonds de Recherche du Quebec – Nature et Technologies (FRQNT).

References

1 A. Krizhevsky, I. Sutskever and G. E. Hinton, Imagenet classification with deep convolutional neural networks, *Adv. Neural Inf. Process. Syst.*, 2012, **25**, 1.
2 Y. LeCun, Y. Bengio and G. Hinton, Deep learning, *Nature*, 2015, **521**, 436.
3 L. D. Harmon, Artificial Neuron, *Science*, 1958, **129**, 962.
4 A. K. Jain, J. Mao and K. M. Mohiuddin, Artificial neural networks a tutorial, *IEEE Comput.*, 1996, **29**, 31.
5 S.-C. Wang, *Interdisciplinary computing in java programming*, Springer, Boston, MA, 2003.
6 A. Krogh, What are artificial neural networks, *Nat. Biotechnol.*, 2008, **26**, 195.
7 D. Beniaguev, I. Segev and M. London, Single cortical neurons as deep artificial neural networks, *Neuron*, 2021, **109**, 2727 e2723.
8 G. R. Yang and X. J. Wang, Artificial Neural Networks for Neuroscientists: A Primer, *Neuron*, 2020, **107**, 1048.
9 W. Zhang, *et al.*, Neuro-inspired computing chips, *Nat. Electron.*, 2020, **3**, 382.
10 M. Le Gallo, *et al.*, A 64-core mixed-signal in-memory compute chip based on phase-change memory for deep neural network inference, *Nat. Electron.*, 2023, **6**, 680.
11 D. Purves, *et al.*, *Neurosciences*, De Boeck Supérieur, 2009.
12 T. Ohno, *et al.*, Short-term plasticity and long-term potentiation mimicked in single inorganic synapses, *Nat. Mater.*, 2011, **10**, 591.
13 K. He, C. Wang, Y. He, J. Su and X. Chen, Artificial Neuron Devices, *Chem. Rev.*, 2023, **123**, 13796.
14 T. Wang, *et al.*, A chemically mediated artificial neuron, *Nat. Electron.*, 2022, **5**, 586.
15 T. Sarkar, *et al.*, An organic artificial spiking neuron for in situ neuromorphic sensing and biointerfacing, *Nat. Electron.*, 2022, **5**, 774.
16 G. S. Syed, Y. Zhou, J. Warner and H. Bhaskaran, Atomically thin optomemristive feedback neurons, *Nat. Nanotechnol.*, 2023, **18**, 1036.
17 Y. Chen, *et al.*, Real-Time, Dual-Physical-Layer Encryption Directly within an Optical Sensor on a Silicon Platform, *ACS Appl. Mater. Interfaces*, 2025, **17**, 28350.
18 T. V. Bliss and T. Lømo, Long–lasting potentiation of synaptic transmission in the dentate area of the anaesthetized rabbit following stimulation of the perforant path, *J. Physiol.*, 1973, **232**, 331.
19 D. Zipser, B. Kehoe, G. Littlewort and J. Fuster, A spiking network model of short-term active memory, *J. Neurosci.*, 1993, **13**, 3406.
20 J. C. Magee, Dendritic Ih normalizes temporal summation in hippocampal CA1 neurons, *Nat. Neurosci.*, 1999, **2**, 508.
21 H. Seung, *et al.*, Integration of synaptic phototransistors and quantum dot light-emitting diodes for visualization and recognition of UV patterns, *Sci. Adv.*, 2022, **8**, eabq3101.
22 J. Chen, *et al.*, Optoelectronic graded neurons for bioinspired in-sensor motion perception, *Nat. Nanotechnol.*, 2023, **18**, 882.
23 Y. Narukawa, M. Ichikawa, D. Sanga, M. Sano and T. Mukai, White light emitting diodes with super-high luminous efficacy, *J. Phys. D: Appl. Phys.*, 2010, **43**, 354002.
24 J. Tombran-Tink and C. J. Barnstable, *Visual transduction and non-visual light perception*, Springer Science & Business Media, 2008.

25 J. M. Fuster and J. P. Jervey, Inferotemporal neurons distinguish and retain behaviorally relevant features of visual stimuli, *Science*, 1981, **212**, 952.
26 B. E. Reese, Developmental plasticity of photoreceptors, *Prog. Brain Res.*, 2004, **144**, 3.
27 Z. Deng, S. Oosterboer and W. Wei, Short-term plasticity and context-dependent circuit function: Insights from retinal circuitry, *Sci. Adv.*, 2024, **10**, eadp5229.
28 S. A. Baccus and M. Meister, Fast and slow contrast adaptation in retinal circuitry, *Neuron*, 2002, **36**, 909.
29 M. F. Vafadar and S. Zhao, Architecture for Surface-Emitting Lasers with On-Demand Lasing Wavelength by Nanowire Optical Cavities, *ACS Nano*, 2024, **18**, 14290.
30 M. F. Vafadar and S. Zhao, Low-Temperature Selective Area Epitaxy of GaN Nanowires: Toward a Top-Surface Morphology Controllable, Fully Epitaxial Nanophotonic Platform, *ACS Appl. Nano Mater.*, 2022, **5**, 16045.
31 M. F. Vafadar and S. Zhao, Photo–Detectable Light–Emitting Devices with Epitaxial Nanowire Photonic Crystals, *Phys. Status Solidi A*, 2025, **23**, 2500157.
32 D. Williams, Eagle eyed or bird brained?, *Eye*, 2023, **37**, 2426.
33 J. González-Martín-Moro, J. L. Hernández-Verdejo and A. Clement-Corral, The visual system of diurnal raptors: Updated review, *Arch. Soc. Esp. Oftalmol.*, 2017, **92**, 225.
34 T. Baden and D. Osorio, The Retinal Basis of Vertebrate Color Vision, *Annu. Rev. Vis. Sci.*, 2019, **5**, 177.
35 S. Zhao, H. P. T. Nguyen, M. G. Kibria and Z. Mi, III-Nitride nanowire optoelectronics, *Prog. Quantum Electron.*, 2015, **44**, 14.
36 S. Zhao, III-Nitride nanostructures: Selective area epitaxy, surface emitting lasers, and emerging photodetectors, *Semicond. Semimetals*, 2024, **116**, 1.
37 S. Nakamura, M. Senoh, N. Iwasa and S.-i. Nagahama, High-Brightness InGaN Blue, Green and Yellow Light-Emitting Diodes with Quantum Well Structures, *Jpn. J. Appl. Phys.*, 1995, **34**, L797.
38 M. Fathabadi, Y. Yin, S. Li and S. Zhao, Breaking the Built–In Electric Field Barrier in p–n Heterojunction for Self–Powered, Wavelength Distinguishable Photoelectrochemical Photodetectors: Toward Low Power Consumption and Secure Underwater Wireless Sensor Network, *Adv. Opt. Mater.*, 2023, **12**, 2302372.
39 X. Hai, R. T. Rashid, S. M. Sadaf, Z. Mi and S. Zhao, Effect of low hole mobility on the efficiency droop of AlGaN nanowire deep ultraviolet light emitting diodes, *Appl. Phys. Lett.*, 2019, **114**, 101104.
40 K. H. Li, X. Liu, Q. Wang, S. Zhao and Z. Mi, Ultralow-threshold electrically injected AlGaN nanowire ultraviolet lasers on Si operating at low temperature, *Nat. Nanotechnol.*, 2015, **10**, 140.
41 M. G. Kibria, *et al.*, Tuning the surface Fermi level on p-type gallium nitride nanowires for efficient overall water splitting, *Nat. Commun.*, 2014, **5**, 3825.
42 S. Zhao, *et al.*, p-Type InN Nanowires, *Nano Lett.*, 2013, **13**, 5509.
43 S. Zhao, Z. Mi, M. G. Kibria, Q. Li and G. T. Wang, Understanding the role of Si doping on surface charge and optical properties: Photoluminescence study of intrinsic and Si-doped InN nanowires, *Phys. Rev. B: Condens. Matter Mater. Phys.*, 2012, **85**, 245313.
44 V. Veeramuthu, *et al.*, Scalable InGaN nanowire micro-LEDs: paving the way for next-generation display technology, *Natl. Sci. Rev.*, 2025, **12**, nwae306.
45 A. Pandey, *et al.*, Toward High Wall-Plug Efficiency in Nanowire-Based Red Micro-LEDs, *ACS Photonics*, 2025, **12**, 4988.